Linear and Bent M(μ-CN)Pt(μ-CN)M Chains: Probes for Remote Metal−Metal Interactions

Guy N. Richardson, Udo Brand, and Heinrich Vahrenkamp*

Institut für Anorganische und Analytische Chemie der Universität Freiburg, Albertstrasse 21, D-79104 Freiburg, Germany

Received December 3, 1998

Cyanide-bridged trinuclear complexes containing square-planar platinum at the center were synthesized and identified by structure determinations. Their chemical building blocks were *cis*- and *trans*-PtL_2X_2, Cp(dppe)FeX, $Cp(PPh_3)_2RuX$ (with X = Hal or CN), $Pt(CN)_4^{2-}$, and $Fe(CN)_6^{3-}$. Several of the intermediate dinuclear complexes were isolated and used for reference purposes. The molecular structures, the ν(CN) IR data, the cyclic voltammograms, and the UV−vis−near-IR spectra were used to probe the effects of the geometry at platinum (cis vs trans), of cyanide−isocyanide isomerism ($Pt(CN)_2$ vs $Pt(NC)_2$), of the nature and ligation of the terminal metals (Fe vs Ru), and of one- or two-electron oxidation. The redox properties and the observed intervalence transfers indicate that there is electronic communication between the outer metal atoms along the linear M−CN chains containing trans-configured platinum, but not along the bent chains containing cis-configured platinum.

The renaissance in the chemistry and physics of polynuclear or polymeric metal cyanides is nourished by application-oriented topics like the design of new magnetic materials[1] or light-harvesting devices,[2] but also by the suitability of $M_x(CN)_y$ building blocks for self-assembly processes.[3] In addition to the well-established variations of the Prussian Blue structure[4] and networks and intercalations based on the cadmium cyanide structure[5] as examples of infinite arrays, the design of molecular entities has yielded aesthetically pleasing star-,[6] ring-,[7] and boxlike[8] oligometallic complexes composed of M−CN−M′ rods linked together at M and M′.

The physical properties of the metal cyanide derived materials (color, conductivity, magnetism) are based on the electronic interactions between adjacent metals mediated through the linear M−CN−M′ bridge. For this reason cyanide-bridged complexes were among the first examples studied for mixed valence and metal−metal charge transfer.[9] The simplest objects of study for long-distance metal−metal interactions in this class of compounds (other than the highly symmetrical solid-state materials) should be oligonuclear complexes with chainlike arrangements of metal atoms and bridging cyanide ions. However, since preparative chemists have not been too active in this field, the number of complexes containing three metal atoms linked this way is still limited,[10] and no such complex containing four metal atoms has been fully characterized yet.

The challenge to start a systematic chemical study of complexes containing $(M-CN)_n$ chains should be rewarded by the chance to obtain systematic information on their metal−metal interactions. Questions to be addressed should be the influences due to the nature of the metals and their ligation, the orientation of the cyanide bridges and the shape of the chains, and their changes brought about by redox interconversions. Some information on long-range metal−metal interactions was obtained for trinuclear complexes by optical spectroscopy[2,11] and cyclic voltammetry.[12] First indications on the influence of the chain shape were found for two similar complexes differing mainly by a cis or trans orientation of the cyanide ligands at a central ruthenium atom.[13] These findings underline the necessity to gain a broader basis for their discussion.

Coming from cluster chemistry we used cyanide initially as a linker between clusters and external organometallic units.[14]

(1) *Magnetic Molecular Materials*; Gatteschi, D., Kahn, O., Miller, J. S., Palacio, F., Eds.; Kluwer Academic Publishers: Dordrecht, 1990; NATO Sci. E, Vol. 98.
(2) Balzani, V.; Juris, A.; Venturi, M.; Campagna, S.; Serroni, S. *Chem. Rev.* **1996**, *96*, 759. Bignozzi, C. A.; Schoonover, J. R.; Scandola, F. *Prog. Inorg. Chem.* **1997**, *44*, 1.
(3) For a collection of recent references, see: Fukita, N.; Ohba, M.; Okawa, H.; Matsuda, K.; Iwamura, H. *Inorg. Chem.* **1998**, *37*, 842.
(4) Ferlay, S.; Mallah, T.; Ouahes, R.; Veillet, P.; Verdaguer, M. *Nature* **1995**, *378*, 701. Entley, W. R.; Girolami, G. S. *Science* **1995**, *268*, 397.
(5) Hoskins, B. F.; Robson, R. *J. Am. Chem. Soc.* **1990**, *112*, 1546. *Chemistry of Pseudohalides*; Clark, R. J. H., Ed.; Elsevier: Amsterdam, 1986.
(6) Fritz, M.; Rieger, D.; Bär, E.; Beck, G.; Fuchs, J.; Holzmann, G.; Fehlhammer, W. P. *Inorg. Chim. Acta* **1992**, *198*, 513. Parker, R. J.; Hockless, D. C. R.; Moubaraki, B.; Murray, K. S.; Spiccia, L. *Chem. Commun.* **1996**, 2789.
(7) Schinnerling, P.; Thewalt, U. *J. Organomet. Chem.* **1992**, *431*, 41. Lai, S. W.; Cheung, K. K.; Chan, M. C. W.; Che, C. M. *Angew. Chem.* **1998**, *110*, 193; *Angew. Chem., Int. Ed.* **1998**, *37*, 182.
(8) Heinrich, J. L.; Berseth, P. A.; Long, J. R. *Chem. Commun.* **1998**, 1231. Klausmeyer, K. K.; Rauchfuss, T. B.; Wilson, S. R. *Angew. Chem.* **1998**, *110*, 1808; *Angew. Chem., Int. Ed.* **1998**, *37*, 1694.
(9) Glauser, R.; Hauser, U.; Herren, F.; Ludi, A.; Roder, P.; Schmidt, E.; Siegenthaler, H.; Wenk, F. *J. Am. Chem. Soc.* **1973**, *95*, 8457. Haim, A.; Wilmarth, W. K. *J. Am. Chem. Soc.* **1961**, *83*, 509.
(10) Vahrenkamp, H.; Geiss, A.; Richardson, G. N. *J. Chem. Soc., Dalton Trans.* **1997**, 3643.
(11) Scandola, F.; Argazzi, R.; Bignozzi, C. A.; Chiorboli, C.; Indelli, M. T.; Rampi, M. A. *Coord. Chem. Rev.* **1993**, *125*, 283 and references therein.
(12) Brown, N. C.; Carpenter, G. B.; Connelly, N. G.; Crossley, J. G.; Martin, A.; Orpen, A. G.; Rieger, A. L.; Rieger, P. H.; Worth, G. H. *J. Chem. Soc., Dalton Trans.* **1996**, 3977 and references therein.
(13) Bignozzi, C. A.; Roffia, S.; Chiorboli, C.; Davila, J.; Indelli, M. T.; Scandola, F. *Inorg. Chem.* **1989**, *28*, 4350. Coe, B. J.; Meyer, T. J.; White, P. S. *Inorg. Chem.* **1995**, *34*, 3600.
(14) (a) Oswald, B.; Powell, A. K.; Rashwan, F.; Heinze, J.; Vahrenkamp, H. *Chem. Ber.* **1990**, *123*, 243. (b) Zhu, N.; Hauser, P.; Heinze, J.; Vahrenkamp, H. *J. Cluster Sci.* **1995**, *6*, 147. (c) Zhu, N.; Appelt, R.; Vahrenkamp, H. *J. Organomet. Chem.* **1998**, *565*, 187.

10.1021/ic981384l CCC: $18.00
Published on Web 06/05/1999

For dinuclear M−CN−M′ complexes we could then demonstrate the influences of redox and cyanide−isocyanide isomerism on structures, spectra, electron transfer properties, and metal−metal charge transfer.[15] Initial studies on similar tri-[16] and tetranuclear complexes[17] indicated that long-range electronic interactions can exist between metal atoms up to 13 Å apart. These findings prompted us to start a broader investigation of M(μ-CN)M′(μ-CN)M″ complexes in which the parameters mentioned above are varied. This paper reports on the first series of such trinuclear complexes. Square-planar platinum(II) was used as the center of the complexes as it is sufficiently inert toward redox changes, ligand substitution, and cis−trans isomerization. Redox-active iron and ruthenium centers were used as the external metals. Cis and trans orientations of the external units at platinum as well as both orientations of the cyanide bridge were realized. The resulting complexes were subjected to structure determinations, IR and UV−vis−near-IR spectroscopy, cyclic voltammetry, and chemical redox reactions.

Results and Discussion

Syntheses. Complexes with Pt−NC Ligations. The preparative procedure to obtain the cyanide-bridged di- or trinuclear complexes was the same throughout: a labile ligand on one metal, usually halide, was replaced by a cyanometal "ligand", bringing in the other metal. Thus, for generating Pt−NC−M arrays the platinum-containing starting materials were **1**, **2a**, and **2b**. The cyanometal "ligands" were **3** and **4** introducing iron and ruthenium in a form which we found suitable for electrontransfer reactions.[15,16] The replacement of chloride by

trans-$(py)_2PtCl_2$ **1** *cis*-(bpy)$PtCl_2$ **2a** *cis*-(phen)$PtCl_2$ **2b**

Cp(dppe)Fe−CN **3** $Cp(PPh_3)_2Ru-CN$ **4**

the cyanometal complex proceeded stepwise in refluxing methanol. The iron reagent **3** turned out to be a much stronger nucleophile. It yielded the dinuclear complexes **5**, **6a**, and **6b** straightforwardly, while with the ruthenium reagent only **7a** was accessible. Furthermore, while **3** produced several trinuclear complexes (see below), **4** did not react with any of the mono- or dinuclear species to form a trinuclear product. An excess of

trans-[Cp(dppe)Fe−CN−$Pt(py)_2$Cl]SbF_6 **5**

cis-[Cp(dppe)Fe−CN−Pt(bpy)Cl]SbF_6 **6a**

cis-[Cp(dppe)Fe−CN−Pt(phen)Cl]SbF_6 **6b**

cis-[$Cp(PPh_3)_2$Ru−CN−Pt(bpy)Cl]SbF_6 **7a**

3 reacted with all three platinum starting complexes to form the trinuclear compounds **8**, **9a**, and **9b**. In these and all other reactions visual inspection allowed control of the reaction proceedings and assessment of the geometry of the reaction products. Just as for the starting materials **1** (yellow) and **2** (red), the products with trans geometry have a deeper color (usually red) than those with cis geometry (usually yellow to orange).

trans-[Cp(dppe)Fe−CN−$Pt(py)_2$−NC−Fe(dppe)Cp]$(SbF_6)_2$ **8**

cis-[{Cp(dppe)Fe−CN}$_2$Pt(bpy)]$(SbF_6)_2$ **9a**

cis-[{Cp(dppe)Fe−CN}$_2$Pt(phen)]$(SbF_6)_2$ **9b**

Complexes with Pt−CN Ligation. In this case cyanide was attached to platinum in the starting materials **10** and **11**, and the labile ligands were attached to iron in the reagents **12** and **13**. We had to resort to **13** as **12** had the tendency to make incomplete reactions and produce too much of the side product mentioned below. Combining **10** and **12** yielded trinuclear **14**.

trans-$(py)_2Pt(CN)_2$ **10** *cis*-(bpy)$Pt(CN)_2$ **11**

Cp(dppe)FeBr **12** [Cp(dppe)Fe(MeCN)]X **13a**: X = SbF_6 **13b**: X = Br

Rather than the expected dinuclear Fe−NC−Pt−CN intermediate of this reaction, complex **15**, resulting from a transfer of the dppe ligand to platinum, was obtained. **15** also resulted when **11** and **13a** were combined, but here the desired trinuclear complex **16** was the main product. In these reactions no evidence of cyanide−isocyanide isomerizations was observed although the reagents were refluxed for extended periods in some cases. The isomeric complexes **8**/**14** and **9a**/**16** and their dinuclear precursors **5** and **6a** are isomerically pure according to IR and NMR spectroscopy.

trans-[Cp(dppe)Fe−NC−$Pt(py)_2$−CN−Fe(dppe)Cp]$(SbF_6)_2$ **14**

cis-[Cp(dppe)Fe−NC−Pt(dppe)CN]SbF_6 **15**

cis-[{Cp(dppe)Fe−NC}$_2$Pt(bpy)]$(SbF_6)_2$ **16**

Complexes Derived from Cyanometalates. In order to reduce the organometallic content of the complexes and to make terminal CN ligands for the planned extension of the chain length available, the cyanometalates $Pt(CN)_4^{2-}$ and $Fe(CN)_6^{3-}$ were tested as building blocks in the form of **17** and **18a**,**b**.

$(PPN)_2[Pt(CN)_4]$ **17** $A_3[Fe(CN)_6]$ **18a**: A = PPN **18b**: A = NBu_4 $Cp(PPh_3)_2RuCl$ **19**

Treatment of **17** with **13b** yielded trinuclear **20**. Starting with tetracyanoplatinate also ruthenium could be incorporated in moderately stable trinuclear complexes. The reaction between **17** and **19** produced **21**. Even the mixed trimetallic compound **22** was accessible by stepwise addition of **12** and **19** to **17**. The intermediate of this reaction, [Cp(dppe)Fe−NC−$Pt(CN)_3]^-$, could be seen forming in solution by the color change from colorless to pink but could not be isolated. Two complexes with

(15) (a) Zhu, N.; Vahrenkamp, H. *J. Organomet. Chem.* **1994**, *472*, C5. (b) Zhu, N.; Vahrenkamp, H. *Angew. Chem.* **1994**, *106*, 2166; *Angew. Chem., Int. Ed. Engl.* **1994**, *33*, 2090. (c) Zhu, N.; Vahrenkamp, H. *Chem. Ber.* **1997**, *130*, 1241.

(16) Zhu, N.; Vahrenkamp, H. *J. Organomet. Chem.*, in press.

(17) Geiss, A.; Keller, M.; Vahrenkamp, H. *J. Organomet. Chem.* **1997**, *541*, 441.

trans-[Cp(dppe)Fe−NC−Pt(CN)$_2$−CN−Fe(dppe)Cp]
20

trans-[Cp(PPh$_3$)$_2$Ru−NC−Pt(CN)$_2$−CN−Ru(PPh$_3$)$_2$Cp]
21

trans-[Cp(dppe)Fe−NC−Pt(CN)$_2$−CN−Ru(PPh$_3$)$_2$Cp]
22

terminal Fe(CN)$_6$ units could be isolated which are somewhat labile and whose identification rests only on analytical and IR data so far. Dinuclear **23** resulted from **1** and **18a**, trinuclear **24** from **1** and **18b**. The choice of cation for the hexacyanoferrate is crucial in these reactions as it allows the separation of **23** and **24** from byproducts and starting materials by crystallization.

trans-[(CN)$_5$Fe−CN−Pt(py)$_2$Cl](PPN)$_2$
23

trans-[(CN)$_5$Fe−CN−Pt(py)$_2$−NC−Fe(CN)$_5$](NBu$_4$)$_4$
24

Besides analyses and NMR spectra the identification of the new complexes rests on FAB-MS which produced the correct molecular masses of the complex ions of **5**, **6a**, **8**, **9a**, **20**, **21**, and **22** as well as on the structure determinations of **5**, **6a**, **8**, **9a**, **14**, **16**, and **20**. There can be little doubt that the assigned orientations of the bridging cyanide ligands which are derived from those in the reagents are correct. The assignments are consistent with previous experience,[15,16] IR data, molecular structures, and redox behavior. Thus the inertness of platinum as well as of the organometallic building blocks has made possible an important feature of this work, the study of influences due to cyanide orientation (Pt−CN−M vs Pt−NC−M).

Structures. The molecular structures of the dinuclear complex cations of *trans*-**5** and *cis*-**6a** serve to define some bonding parameters for reference purposes. Figures 1 and 2 give the information. Noteworthy are the near to ideal square-planar coordination of platinum, the small variance of the C−N bond length in comparison to monodentate CN$^-$,[18] the close to linear Fe−C−N arrangement and the significant bending of the Pt−N−C arrangement. The different degrees of bending of M−C−N vs M−N−C are common to most cyanide-bridged complexes; see also below. They reflect the different degrees of π-back-bonding at the C and N termini of the CN bridge.

The effects of cyanide−isocyanide isomerism can be seen by comparing the structures of **8** and **14**; see Figures 3 and 4. Both complexes are centrosymmetrical with platinum on an inversion center, but not isomorphous. Both have similar, though not identical, shapes, as seen in the figures. They differ significantly in their Pt(μ-C−N)Fe arrays. This array is more "normal" for Fe−C−N−Pt in **8** being comparable to that in **5** and **6a**, i.e., the Fe−C bond is rather short and Pt−N−C shows more bending than Fe−C−N. The situation in **14** is unusual at first glance: while the Fe−N bond is typically longer than the Fe−C bond in **8**, the Pt−C bond is not shorter, but longer than the Pt−N bond in **8**. Likewise in **14** the Fe−N−C array is hardly more bent than the Pt−C−N array. Both these observations mean that Pt−C π-bonding is unusually weak and Fe−N π-bonding unusually strong in **14**. An explanation for this may be found in the well-known strong trans effect of cyanide at

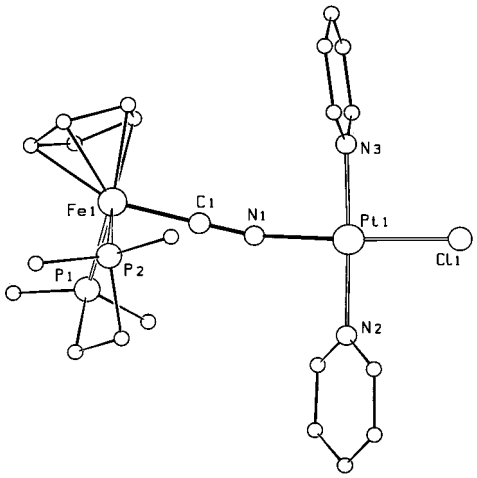

Figure 1. Structure of the cation of complex **5** (phenyl groups omitted for clarity). Important bond lengths (Å) and angles (deg): Fe−C 1.851(9), C−N 1.15(1), Pt−N1 1.978(8), Pt−N2 2.040(7), Pt−N3 2.018(7), Pt−Cl 2.27(4), Fe−P(av) 2.185(4), Fe−C−N 175.4(7), Pt−N−C 166.7(7).

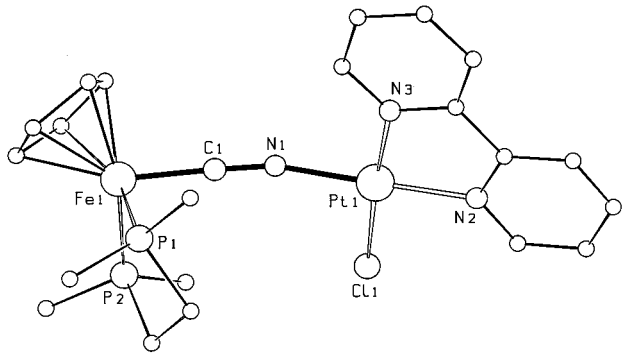

Figure 2. Structure of the cation of complex **6a** (phenyl groups omitted for clarity). Important bond lengths (Å) and angles (deg): Fe−C 1.857(6), C−N 1.160(6), Pt−N1 1.968(5), Pt−N2 2.005(4), Pt−N3 2.012(5), Pt−Cl 2.279(2), Fe−P(av) 2.191(3), Fe−C−N 174.4(5), Pt−N−C 166.1(5).

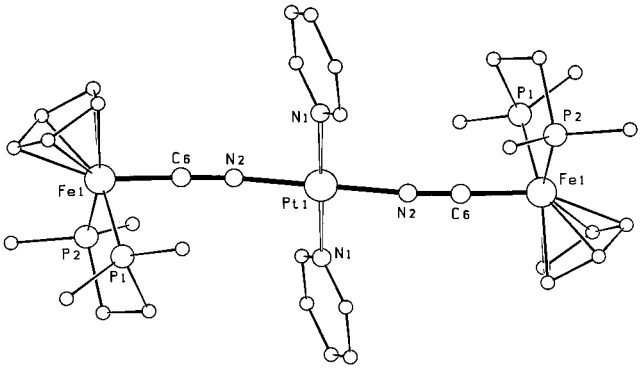

Figure 3. Structure of the centrosymmetrical cation of complex **8** (phenyl groups omitted for clarity). Important bond lengths (Å) and angles (deg): Pt−N1 2.026(4), Pt−N2 1.956(5), C−N 1.176(7), Fe−C 1.839(6), Fe−P(av) 2.177(2), Pt−N−C 166.9(4), Fe−C−N 176.4(4).

platinum(II). A cyanide ligand weakens the Pt−cyanide bond trans to it, as can be seen by comparing Ba[Pt(CN)$_4$] or *trans*-[(amine)$_2$Pt(CN)$_2$] (Pt−C$_{average}$ = 1.99 Å)[19] with *cis*-[(bpy)Pt(CN)$_2$] or *cis*-[(bipyrimidine)Pt(CN)$_2$] (Pt−C$_{average}$ = 1.95 Å).[20] The internal reference for this is complex **16** (see below), which

(18) Sharpe, A. G. *The Chemistry of Cyano Complexes of the Transition Metals*; Academic Press: New York, 1976. Golub, A. K.; Köhler, H.; Skopenko, V. V. In *Chemistry of Pseudohalides*; Clark, R. J. H., Ed.; Elsevier: Amsterdam, 1986; pp 77−85.

(19) (a) Maffly, R. L.; Johnson, P. L.; Williams, J. M. *Acta Crystallogr., Sect. B* **1977**, *B33*, 884. (b) Babkov, A. V.; Potekhin, K. A.; Struchkov, Y. T. *Zh. Neorg. Khim.* **1996**, *41*, 1128.

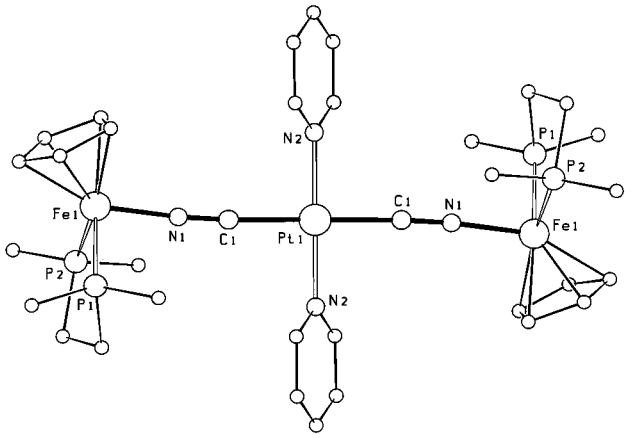

Figure 4. Structure of the centrosymmetrical cation of complex **14** (phenyl groups omitted for clarity). Important bond lengths (Å) and angles (deg): Pt−N 2.020(5), Pt−C 1.980(6), C−N 1.149(7), Fe−N 1.903(5), Fe−P(av) 2.212(4), Pt−C−N 176.8(6), Fe−N−C 175.3(5).

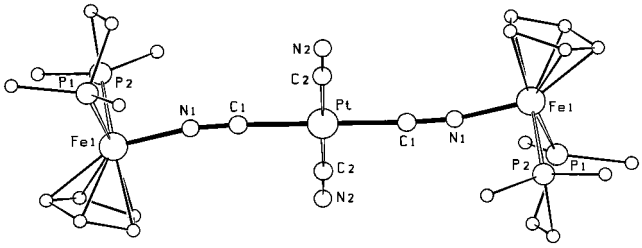

Figure 5. Molecular structure of the centrosymmetrical complex **20** (phenyl groups omitted for clarity). Important bond lengths (Å) and angles (deg): Pt−C1 1.993(6), Pt−C2 1.990(8), C1−N1 1.131(8), C2−N2 1.153(10), Fe−N1 1.914(5), Fe−P(av) 2.207(4), Pt−C1−N1 176.0-(6), Pt−C2−N2 178.8(7), Fe−N1−C1 168.5(5).

indeed has a more "normal" bonding situation for the cis-configured Pt−C−N−Fe units. In essence the weakening of the Pt−C bonds in **14** due to the mutual trans effect strengthens the Fe−N bonds and makes the Pt−C−N−Fe array in this case more rigid than all Pt−N−C−Fe arrays and also the Pt−C−N−Fe array in cis-configured **16**.

The structure of complex **20** is a variation of that of **14**; see Figure 5. Like **8** and **14**, **20** is centrosymmetrical. Its terminal cyanide ligands can serve as a reference for the trans effect as well as for the effects of attaching a second metal at the N terminus. The trans effect is quite noticeable: both terminal and bridging cyanide have rather long Pt−C bonds (see above). There seems to be no influence of the iron attachment on the Pt−C distance. This time there is a more typical degree of bending at the cyanide's C and N termini: while all four Pt−C−N arrays are close to linearity, the Fe−N−C array is bent as in other Fe−N−C−M complexes.[15,16]

Complexes **9a** and **16** are the cyanide/isocyanide couple of the cis-configured trinuclear complexes; cf. Figures 6 and 7. **9a** crystallizes with two molecules in the asymmetric unit which differ in the orientations of the dppe's phenyl rings. As a result there are several values for each bond or angle in the Pt(μ-C−N)Fe units which actually show a significant spread. The average values, however, show the expected magnitudes and trends. First, Pt−C in **16** is typically shorter than Pt−N in **9a**, and likewise Fe−C in **9a** is shorter than Fe−N in **16**. Second, due to the absence of a trans effect Pt−C in **16** is also much shorter than in **14** and **20**, but Pt−N in **9a** is not much different from

(20) (a) Connick, W. B.; Henling, L. M.; Marsh, R. E. *Acta Crystallogr., Sect. B* **1996**, *B52*, 817. (b) Biedermann, J.; Gliemann, G.; Klement, U.; Range, K. J.; Zabel, M. *Inorg. Chem.* **1990**, *29*, 1884.

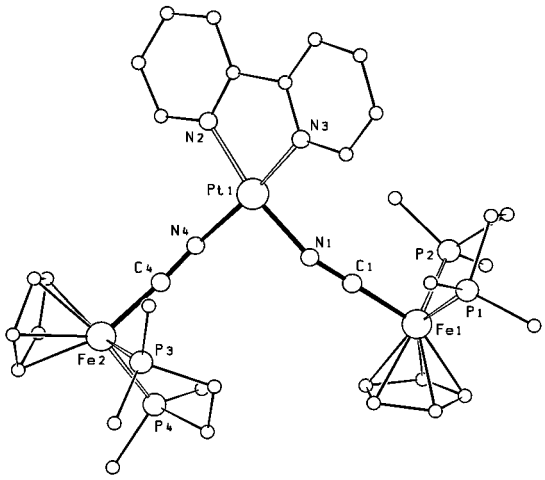

Figure 6. Structure of the cation of complex **9a** (phenyl groups omitted for clarity). Important bond lengths (Å) and angles (deg): Pt−N(bpy) 1.97−2.00(1), av 1.99; Pt−N(CN) 1.97−1.99(1), av 1.98; C−N 1.18−1.19(2), av 1.18; Fe−C 1.82−1.85(2), av 1.84; Fe−P 2.18−2.21(1), av 2.19; Fe−C−N 172.8−178.1(14), av 175.7; Pt−N−C 149.7−169.5-(12), av 157.6.

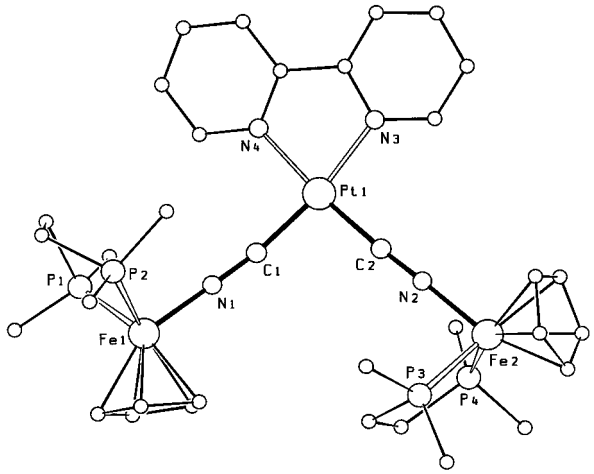

Figure 7. Structure of the cation of complex **16** (phenyl groups omitted for clarity). Important bond lengths (Å) and angles (deg): Pt−N(bpy) 2.03−2.05(1), Pt−C 1.90−1.91(1), C−N 1.18−1.24(2), Fe−N 1.89−1.92(2), Fe−P 2.19−2.23(1), Pt−C−N 166.9 and 176.6(1), Fe−N−C 1.75.1 and 177.2(1).

Pt−N in **8**. Third, in **9a** the Fe−C−N array is reasonably close to linearity, while the Pt−N−C array is severely bent (down to 150°). The only deviation from these "normal" findings occurs for the bending of Fe−N−C and Pt−C−N in **16**: as in **14** the bending is small for both arrays, and Pt−C−N is actually a little more bent than Fe−N−C. It seems reasonable to assume that in some of these complexes packing forces modify the electronic effects on the M−C−N or M−N−C arrays which have characteristically small deformation force constants.

Altogether the structure determinations have confirmed not only the molecular shapes of the trinuclear complexes but also the assumed orientations of the cyanide ligands between platinum and iron. The general trends of M−C and M−N bond lengths and their relation to metal−cyanide π-bonding and deformation of the M−C−N−M′ array, as learned from dinuclear complexes, are confirmed. Cis−trans isomerism at the central metal atom and cyanide−isocyanide isomerism in the molecular chain are established, providing solid structural information for the discussion of the spectroscopic and electrochemical data.

Table 1. IR Data[a]

complex	backbone	CN_{bridge}	$CN_{term.}$
	Mononuclear Reagents		
3	Fe−CN		2065
4	Ru−CN		2072
10	*trans*-Pt$(CN)_2$		2122
11	*cis*-Pt$(CN)_2$		2144/2134
17	Pt$(CN)_4$		2124
18b	Fe$(CN)_6$		2096
	Dinuclear Complexes		
5	Fe−CN−Pt	2097	
6a	Fe−CN−Pt	2086	
6b	Fe−CN−Pt	2087	
7a	Ru−CN−Pt	2095	
15	*cis*-Fe−NC−Pt−CN	2156	2142
23	$(CN)_5$Fe−CN−Pt	2157	2109
	Trinuclear Complexes		
8	*trans*-Pt$(NC-Fe)_2$	2081	
9a	*cis*-Pt$(NC-Fe)_2$	2092/2067	
9b	*cis*-Pt$(NC-Fe)_2$	2072/2068	
14	*trans*-Pt$(CN-Fe)_2$	2156	
16	*cis*-Pt$(CN-Fe)_2$	2156/2148	
20	*trans*-$(NC)_2$Pt$(CN-Fe)_2$	2147	2128
21	*trans*-$(NC)_2$Pt$(CN-Ru)_2$	2153	2132
22	*trans*-$(NC)_2$Pt−(CN−Fe)(CN−Ru)	2135	2135
24	*trans*-Pt$\{NC-Fe(CN)_5\}_2$	2158	2116

[a] KBr, $\tilde{\nu}$(CN) in cm^{-1}.

IR Data. The IR data for the CN stretching band are listed in Table 1 for all complexes. Upon coordination of a second metal to a terminal CN ligand in the mononuclear starting materials the CN band position is raised in all cases. This confirms the well-known information that the kinematic effect (i.e., the constraint of the CN motion by double attachment) is the dominating one in determining $\tilde{\nu}$(CN) for bridging cyanide. In comparison the variance within groups containing the same building blocks (e.g., complex **3** in **5**, **6a**, **6b**, **8**, **9a**, **9b** or the inverse complex Cp(dppe)Fe−NC in **14**, **15**, **16**, **20** or complex **18b** in **23** and **24**) is small. This means that the cis or trans orientation at the platinum center cannot be deduced from the positions of the $\tilde{\nu}$(CN) bands. However, all cis-configured complexes show two bands, as expected from symmetry considerations. Within the pairs of CN/NC isomers **8**/**14** and **9a**/**16** the Pt−C bound species have dramatically higher $\tilde{\nu}$(CN) values than the Fe−C bound species. This phenomenon, which is also observed for their mononuclear precursors **3** and **10**/**11**, sheds light on the π-bonding capabilities of Fe, Pt, C, and N in these complexes: it is only the M−C link that experiences significant π-back-donation, and the Cp(dppe)Fe unit is a much better π-donor than any PtL_2 unit. This way the Cp(dppe)Fe units can be identified as those which most easily undergo one-electron oxidations, specifically when bound to the N terminus of bridging cyanide.

Electrochemistry. Of the complexes described here all those containing Cp(dppe)Fe or Cp$(PPh_3)_2$Ru units showed reversible one-electron oxidations, one for the dinuclear and two for the trinuclear compounds. Their redox potentials, as obtained from cyclic or square-wave voltammetry, are listed in Table 2. Details of the electrochemical procedures are given in the Experimental Section.

Upon coordination to platinum the redox potentials of the mononuclear metallocyanides **3** and **4** are raised by 0.3−0.4 V. This holds for the dinuclear (**5**, **6**, **7**) as well as for the trinuclear complexes (**8**, **9**). It must be explained by a net electron flow to the L_2Pt^{II} center, which unlike the organometallic centers $(CO)_5Cr$ and Cp$(CO)_2Mn$[15c] is a good σ-acceptor. In the di- and trinuclear complexes, as in the mononuclear precursors, the ruthenium center is 0.3 V more difficult to oxidize than the iron center. This corresponds to experience[14−16] and helps to make sure that the electron transfers occur at Fe and Ru rather than at Pt. Inverting the orientation of the cyanide-bridge (i.e., from Fe−CN−Pt to Fe−NC−Pt etc., cf. **5**/**15**, **8**/**14**, and **9a**/**16**) decreases the redox potential by 0.2−0.3 V, in accord with the fact that the species to be oxidized, the Cp(dppe)Fe center, becomes much more electron-rich when coordinated to the CN's N terminus, which is a much weaker π-acceptor than the C terminus. All these observations and explanations are in accord with the conclusions drawn above from the ν(CN) data.

Table 2. Electrochemical Data[a]

complex	backbone	$E_{1/2}$(Ox1)	$E_{1/2}$(Ox2)
	Mononuclear Reference Compounds		
3	Fe−CN	0.48	
4	Ru−CN	0.79	
	Dinuclear Complexes		
5	Fe−CN−Pt	0.79	
6a	Fe−CN−Pt	0.85	
6b	Fe−CN−Pt	0.83	
7a	Ru−CN−Pt	1.11	
15	*cis*-Fe−NC−Pt−CN	0.56	
	Trinuclear Complexes		
8	*trans*-Pt$(NC-Fe)_2$	0.79	0.86
9a	*cis*-Pt$(NC-Fe)_2$	0.90 (2e)	
9b	*cis*-Pt$(NC-Fe)_2$	0.86 (2e)	
14	*trans*-Pt$(CN-Fe)_2$	0.52	0.58
16	*cis*-Pt$(CN-Fe)_2$	0.58 (2e)	
20	*trans*-$(NC)_2$Pt$(CN-Fe)_2$	0.36	0.47
21	*trans*-$(NC)_2$Pt$(CN-Ru)_2$	0.89	0.99
22	*trans*-$(NC)_2$Pt(CN−Fe)(CN−Ru)	0.39	1.02

[a] Measured in CH_2Cl_2, potentials in V vs. Ag/AgCl, scan speed 100 mV/s.

The most important observation in the voltammograms was the occurrence of two oxidative waves for four of the symmetrical trinuclear complexes (**8**, **14**, **20**, **21**), which are separated by 60−120 mV. This occurred only and without exception for the species containing linear $[M-CN]_x$ arrays, i.e., for trans-configured platinum. It reveals an electronic interaction between the distant redox centers (Fe or Ru). This interaction is strong enough to be observed electrochemically only for the trans complexes although their redox centers are farther apart (10 Å) than their equivalents in the cis-configured complexes **9** and **16** (7 Å). It indicates that the pathway of the remote metal−metal interaction is the π-bonding system of the $[M-CN]_x$ chains, reminiscent of trans interactions in the chemistry of divalent platinum. The potential difference of the two slightly separated oxidation steps is independent of the orientation of the cyanide bridge; cf. **8** and **14**. It is of the same order of magnitude as that observed by Connelly[21] and ourselves[16] for cyanide-bridged trinuclear systems with tetrahedrally coordinated metal atoms in the center. It implies that the linear trinuclear complexes after oxidation to the M(III)∼Pt(II)∼M(II) species are mixed-valent compounds of weakly delocalized nature to be grouped in class II of the Robin and Day classification.[22]

Preparative Redox Chemistry. Following the electrochemical measurements we tried to obtain the singly oxidized trinuclear complexes and their dinuclear equivalents on a preparative scale by chemical oxidation. To this end dichlo-

(21) (a) Connelly, N. G.; Lewis, G. R.; Moreno, M. T.; Orpen, A. G. *J. Chem. Soc., Dalton Trans* **1998**, 1905. (b) Connelly, N. G.; Hicks, O. M.; Lewis, G. R.; Orpen, A. G.; Wood, A. J. *Chem. Commun.* **1998**, 517.

(22) Robin, M. B.; Day, P. *Adv. Inorg. Chem. Radiochem.* **1967**, *10*, 247.

Table 3. IR Data of Oxidized Complexes[a]

complex	backbone	CN_{bridge}
$[\mathbf{5}]^+$	Fe(III)−CN−Pt(II)	2139
$[\mathbf{8}]^+$	*trans*-Fe(III)−CN−Pt(II)−NC−Fe(II)	2106/2084
$[\mathbf{8}]^{2+}$	*trans*-Fe(III)−CN−Pt(II)−NC−Fe(III)	2111
$[\mathbf{9a}]^{2+}$	*cis*-Fe(III)−CN−Pt(II)−NC−Fe(III)	2127/2100
$[\mathbf{14}]^+$	*trans*-Fe(III)−NC−Pt(II)−CN−Fe(II)	2156/2142
$[\mathbf{14}]^{2+}$	*trans*-Fe(III)−NC−Pt(II)−CN−Fe(III)	2142
$[\mathbf{16}]^{2+}$	*cis*-Fe(III)−NC−Pt(II)−CN−Fe(III)	2171/2154
$[\mathbf{20}]^+$	*trans*-Fe(III)−NC−Pt(II)−CN−Fe(II)[b]	2164/2148
$[\mathbf{20}]^{2+}$	*trans*-Fe(III)−NC−Pt(II)−CN−Fe(III)[c]	2169
$[\mathbf{22}]^+$	*trans*-Fe(III)−NC−Pt(II)−CN−Ru(II)[d]	2182/2155

[a] CH_2Cl_2, $\tilde{\nu}$(CN) in cm^{-1}. [b] $\tilde{\nu}(CN_{term.}) = 2132$. [c] $\tilde{\nu}(CN_{term.}) = 2134$. [d] $\tilde{\nu}(CN_{term.}) = 2140$.

romethane solutions of the complexes were treated with the oxidizing agents ferrocenium hexafluorophosphate, acetylferrocenium tetrafluoroborate, and $[(4\text{-}BrC_6H_4)_3N]SbF_6$ (magic blue) which in dichloromethane have redox potentials of 0.39, 0.66, and 1.0 V vs Ag/AgCl, respectively.[23] This allowed the oxidation of all complexes containing N-bound Fe(dppe)Cp units and of some complexes containing C-bound Fe(dppe)Cp units, but no oxidation of a $Ru(PPh_3)_2Cp$ center. Following redox titrations with IR and CV measurements showed that the only oxidation products are the one- and two-electron-oxidized species observed by CV before. They are assigned as Fe(III)∼Pt(II) for the dinuclear and as Fe(III)∼Pt(II)∼M(II) or Fe(III)∼Pt(II)∼Fe(III) for the trinuclear complexes. According to the redox titrations the oxidations were complete after addition of 1 or 2 equiv of the oxidant, which could also be verified by observing the distinctive bands of the oxidants (when present in excess) in the visible spectra. Thus convincing evidence for the existence of the singly and doubly oxidized complexes was accumulated. Our attempts to isolate them after addition of appropriate counterions were, however, met with failure.

The IR data of the oxidized complexes (Table 3) confirm the given assignments. As expected, $\tilde{\nu}$(CN) rises upon oxidation of a C-bound Fe(dppe)Cp unit; see **5**, **8**, and **9a**. This is due to reduced π-back-donation from iron to cyanide which depletes the antibonding π^* orbital of the cyanide ion and strengthens the C≡N bond. Conversely one would have expected a significant decrease of $\tilde{\nu}$(CN) upon oxidation of a N-bound Fe(dppe)Cp unit,[15c,16] due to increased π-back-donation from the metal bound at the C terminus. This is not the case here. Only for **14** is a slight decrease of $\tilde{\nu}$(CN) observed, while **16**, **20**, and **22** show an increase upon oxidation. It must be concluded that in these complexes of the two oxidation-related effects (stronger N→Fe π-donation strengthening C≡N and increased Pt→C π-back-donation weakening C≡N) the former is more pronounced. This in turn is in accord with the fact, already mentioned above, that the L_2Pt^{II} center is a relatively weak π-donor in comparison to the previously investigated[14−16] low-valent organometallic units. The rather high $\tilde{\nu}$(CN) values for the platinum cyanides **10** and **11** point in the same direction.

At this point it is worth mentioning that the structural assignments concerning the orientation of the bridging cyanide ligands (CN vs NC) as deduced from the preparations are consistent with the structural and IR data of the complexes as well as with their redox potentials and IR data after oxidation. The integrity of the cyanide orientations is also implied in the subsequent discussion of metal-to-metal charge transfer and mixed-valence phenomena of the oxidized complexes which were not isolated as analytically pure compounds.

(23) Connelly, N. G.; Geiger, W. E. *Chem. Rev.* **1996**, *96*, 877.

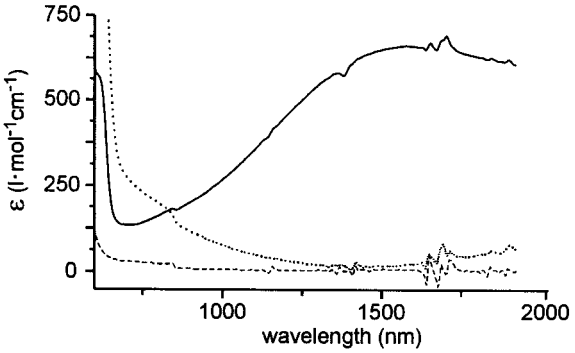

Figure 8. Electronic spectra of **20** and its oxidation products in the near-IR range (in CH_2Cl_2). (See Experimental Section for the irregularities in the spectral traces.)

Electronic Spectra. All oxidized complexes and their precursors were subjected to UV−vis−near-IR spectroscopy, details of which are given in the Experimental Section. Neither of the simple cyanide complexes **10**, **11**, **17**, and **18** shows mentionable spectral features beyond 500 nm, and the organometallic building blocks Cp(dppe)Fe and $Cp(PPh_3)_2Ru$ give rise to only moderately intense absorptions in the visible range. Thus the visible and near-infrared range allowed an unobscured view of possible charge transfer bands. Unfortunately this view was blocked when the strongest oxidant, magic blue, had to be used, as its reactions produced species with intense absorptions across the entire near-IR region. This precluded the investigation of **8** and **9a** and their comparison with their CN/NC isomers **14** and **16**.

The Fe(III)-containing dinuclear complexes $[\mathbf{5}]^+$ and **23** provided the reference measurements. Just like the unoxidized complex **5**, they show intense absorptions in the 250−350 nm range. For $[\mathbf{5}]^+$ the tail of these absorptions in the 400−600 nm range has risen in height by about a factor of 2, and for **23** a weak absorption at 430 nm is observed. None of these features can be interpreted as arising from Pt(II)→Fe(III) charge transfer, confirming that the platinum(II) center in these complexes is inert toward photoinduced oxidation by metal-to-metal charge transfer (MMCT) or intervalence transfer (IT).

In contrast, redox titration of the trans-configured complex **14** with acetylferrocenium tetrafluoroborate leads to the evolution of a medium-intensity IT band at 1313 nm which rises until 1 equiv of the oxidant has been added. This band, assigned to a long-range MMCT in $[\mathbf{14}]^+$ from Fe(II) to Fe(III), decreases upon further addition of oxidant and vanishes when 2 equiv has been added. No such observation is made for the analogous cis-configured complex **16**. The only changes observable during stepwise oxidation from **16** to $[\mathbf{16}]^{2+}$ concern weak features in the visible range, in accord with a color change of the solution from purple to orange. Thus there is also no evidence for a mixed-valent species $[\mathbf{16}]^+$ from the electronic spectra, and the only identifiable IT absorption results from an Fe(II)→Fe(III) MMCT in *trans*-$[\mathbf{14}]^+$ identified as an Fe(III)∼Pt(II)∼Fe(II) species.

The conclusions reached above are borne out by the electronic spectra taken during oxidations of the two trans-configured complexes **20** and **22**. Figure 8 demonstrates that **20** behaves like **14**, in that the successive evolution and decay of an IT band in the near-IR can be observed during the addition of 2 equiv of acetylferrocenium tetrafluoroborate. Fortuitously the generation of only $[\mathbf{20}]^+$ can be achieved with ferrocenium hexafluorophosphate, due to the fact that the redox potential of the latter in dichloromethane (0.39 V) falls right between the redox potentials of **20** (0.36 V) and $[\mathbf{20}]^+$ (0.47 V). When

Table 4. IT Analysis According to the Hush Model

complex	ν_{max} (cm^{-1})	$(\Delta\nu_{1/2})_o$[a] (cm^{-1})	ΔE_o[b] (cm^{-1})	$(\Delta\nu_{1/2})_c$[a] (cm^{-1})	α^2 [c]	λ_{fc}[d] (cm^{-1})
$[\mathbf{14}]^+$	7620	5200	480	4050	0.0008	7140
$[\mathbf{20}]^+$	6410	4720	890	3560	0.0010	5520
$[\mathbf{22}]^+$	13300	[e]	5100	4300	0.0004	8200

[a] Observed (o) and calculated (c) half-widths of the MMCT bands: $(\Delta\nu_{1/2})_c = [2300(\nu_{max} - \Delta E_o)]^{1/2}$. [b] Calculated from the redox potentials $E_{1/2}$ (in V) as $\Delta E_o = 8064\Delta E_{1/2}$. [c] Calculated as $\alpha^2 = 4.24 \times 10^4[(\epsilon_{max}\Delta\nu_{1/2})/(G\nu_{max}R^2)]$, with the degeneracy $G = 2$ for **14** and **20** and $G = 1$ for **22**, with distance $R = 10$ Å. [d] Reorganization energy, calculated from $E_{op} = \lambda_{fc} + \Delta E_o$ with E_{op} = observed energy of the MMCT band. [e] Unaccessible as the MMCT band of $[\mathbf{22}]^+$ is a shoulder on a stronger absorption in the visible range.

ferrocenium hexafluorophosphate is used, the IT band at 1560 nm persists upon addition of 2 equiv of the oxidant. In the spectrum obtained for $[\mathbf{20}]^{2+}$ (dotted line in Figure 8) the weak absorption in the visible and near-IR range is due not to $[\mathbf{20}]^{2+}$ but to acetylferrocene and acetylferrocenium.

Preparative oxidation of **22** could only be performed at the iron center leading to the mixed-valent Fe(III)∼Pt(II)∼Ru(II) species $[\mathbf{22}]^+$. This gives rise to an IT band at 750 nm. The high energy of this band in comparison to that of $[\mathbf{20}]^+$ supports the given assignment: ruthenium is much harder to oxidize in these complexes than iron, and hence Ru(II)→Fe(III) MMCT should require more energy as well. Thus there is a consistent description of long-range MMCT in these trinuclear complexes. Actually $[\mathbf{14}]^+$, $[\mathbf{20}]^+$, and $[\mathbf{22}]^+$ constitute the first cases of unequivocal remote IT in cyanide-bridged trinuclear complexes.[24]

Correlations. Having established unambiguously the remote IT in the three complexes, we could subject it to a semiquantitative treatment. Table 4 lists the relevant data. Using the approximative procedure outlined by Hush[25] and successfully used for related IT systems,[26] the ΔE_o value, the energy difference between the initial and final stages of the MMCT process, can be obtained from the redox potential difference $\Delta E_{1/2}$ (e.g., for **14** and $[\mathbf{14}^+]$), and the E_{op} value, the total MMCT energy, is taken as the energy of the IT band in the near-IR. A test of the validity of this approach is the calculation of the half-widths of the IT bands using the approximate formulas given at the bottom of Table 4. Their agreement with the observed half-widths is in the same range as observed for the related IT systems.[26] As a result of the approximative calculations, the pertinent parameters α^2, the electron delocalization parameter, and λ_{fc}, the reorganization energy, are also obtained.

The data listed in Table 4 classify the trinuclear complexes as typical class II mixed-valence compounds according to the classification of Robin and Day.[22] The correlation between ν_{max} and $\Delta\nu_{1/2}$ is reasonable, and the IT energies are related to the redox potentials of the individual redox centers (see reference compounds in Table 2). The α^2 values come out rather small, specifically when compared to those of dinuclear cyanide-bridged complexes with the same redox centers.[15] Considering the 10 Å distance between the interacting metal atoms and the fact that this distance appears squared in the denominator of the equation for evaluation of α^2, they are, however, in an established range. The calculated values of ΔE_o are small, implying, as expected, that the observed MMCT energy depends almost entirely on the reorganization energy. This is also borne out by the solvatochromic effect observed for the spectra of $[\mathbf{20}]^+$; see Table 5. The MMCT requires more energy in more polar solvents, which implies that the ground state of the transition is more stabilized by solvation than the excited state. The size of the solvatochromic effect, ca. 60 cm^{-1}/DN (DN = solvent donor number[27]), is about half that of similar dinuclear complexes,[15c,28] which may be an expression of the larger distance between the redox centers in **20**.

Table 5. Solvent Dependency of the MMCT Transition of Complex $[\mathbf{20}]^+$

solvent	DN[a]	λ_{max} (nm)	λ_{max} (cm^{-1})
CH_2Cl_2	1.0	1560	6410
CH_3CN	14.1	1410	7092
acetone	17.0	1313	7616

[a] Solvent donor number.[27]

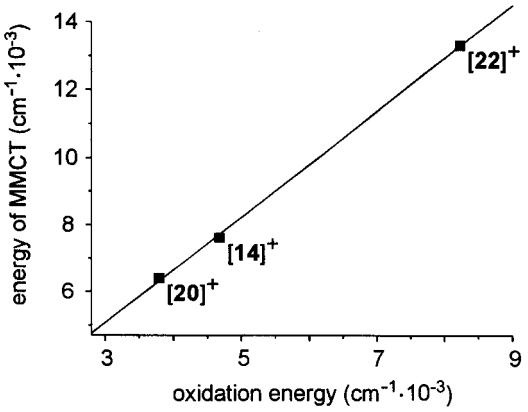

Figure 9. Dependency of the MMCT energies upon the redox potentials of the electron donor groups.

The final argument for remote metal−metal interactions in these complexes lies in the linear relation between the MMCT energy and the redox potential of the donating metal center within the trinuclear complexes. The latter can be taken as the second redox potential of the complexes, e.g., 0.58 V for **14**, the justification for this being that the unit which is reduced during MMCT is identical in all three complexes, namely, a N-bound Cp(dppe)Fe unit. Figure 9 shows the linear relation.

Conclusions

Synthetic procedures for cyanide-bridged trinuclear complexes of the AB_2 type with PtL_2 units in the center (A) and $CpFeL_2$ and $CpRuL_2$ units on the outer positions (B) including cis and trans configurations as well as cyanide and isocyanide ligation at the central platinum(II) centers have been developed, and the resulting structures were confirmed by structure determinations. The structures and the $\tilde{\nu}$(CN) IR data show how the bonding alternatives influence the donor−acceptor properties of the bridging cyanide ligands and the net flow of electron density between two metal atoms mediated by them. The cyclic voltammograms indicate that only in trans-configured complexes is there an electronic interaction between the external metal atoms, as evidenced by a splitting of the redox waves. This is unlike the situation in other oligonuclear cyanide-bridged complexes where, for instance, this interaction is also observed when cis-configured octahedral ruthenium[24,28] or tetrahedral

(24) In the previously reported cases local IT (from the outer metals to the central metal) was the dominating process: Bignozzi, C. A.; Roffia, S.; Scandola, F. *J. Am. Chem. Soc.* **1985**, *107*, 1644. Bignozzi, C. A.; Paradisi, C.; Roffia, S.; Scandola, F. *Inorg. Chem.* **1988**, *27*, 408.
(25) Hush, N. S. *Prog. Inorg. Chem.* **1967**, *8*, 391.
(26) (a) Laidlaw, W. M.; Denning, R. G. *J. Chem. Soc., Dalton Trans.* **1994**, 1987. (b) Sato, M.; Hayashi, Y.; Kumakura, S.; Shimizu, N.; Katada, M.; Kawata, S. *Organometallics* **1996**, *15*, 721.
(27) Marcus, Y. *Chem. Soc. Rev.* **1993**, *22*, 409.
(28) Laidlaw, W. M.; Denning, R. G. *Inorg. Chim. Acta* **1996**, *248*, 51.

units such as $ZnBr_2$[21] are involved. In those cases where preparative oxidation of the AB_2 type complexes is possible, UV−vis−near-IR spectroscopy confirms the long-range metal−metal interactions: intervalence transfer bands in the near-IR are observed only for the trans-configured complexes and only after one-electron oxidation. The dependency of the IT energies upon the redox potentials of the nonoxidized B units in the $[AB_2]^+$ complexes completes the evidence for metal−metal charge transfer along the linear $[M-CN]_x$ chains of 10 Å length.

Experimental Section

The general experimental and measuring techniques were as described previously.[15c] The platinum complexes **1**,[29] **2a**,[30] **2b**,[31] **10**,[32] **11**,[33] and **17**[34] were prepared as published; the preparations of the iron- and ruthenium-containing starting materials are listed in ref 15c. ^{1}H NMR data were recorded on a Bruker AC 200 machine in acetone-d_6; shifts are given in parts per million vs internal TMS, and coupling constants are given in hertz.

Voltammograms were obtained on an Amel-5000 system using Ag/AgCl as reference electrode. The counter and working electrodes were platinum; 10^{-3} M solutions in CH_2Cl_2 were measured. The electrolyte was tetra-*n*-butylammonium hexafluorophosphate (35 mg/mL). Ferrocene ($E_{1/2}$ = +0.39 V vs Ag/AgCl) and cobalticinium hexafluorophosphate (−0.94 V) were used as internal standards. Electrochemical reversibility was verified for all tabulated redox steps by ΔE_p values of ca. 60 mV. This holds also for the two-electron transitions which were identified as such by their peak currents which for the same complex concentrations were about twice those of the one-electron transitions.

UV−vis−near-IR spectra were recorded with a Jasco UV 570 spectrometer with a measuring range of 200−2500 nm. Samples were ca. 3×10^{-4} M in CH_2Cl_2. The relatively low absorptivities of the MMCT bands beyond 1000 nm required a high gain of the spectrometer. This made the irregularities of the baseline in the near-IR range visible; cf. Figure 8.

5. A solution of **1** (200 mg, 0.47 mmol), **3** (257 mg, 0.47 mmol), and $NaSbF_6$ (122 mg, 0.47 mmol) in methanol (120 mL) was heated to reflux for 24 h. After cooling to room temperature the solution was filtered to remove traces of **8**. After evacuation of the filtrate to dryness the residue was picked up in a minimum amount of CH_2Cl_2. Chromatography over a 2 × 15 cm silica gel column with CH_2Cl_2/acetone (5:2) afforded from the single, yellow band 330 mg (75%) of **5** as yellow crystals, mp 242 °C (dec). ^{1}H NMR: 1.98−2.00 [m, 2H, C_2H_4], 2.33−2.37 [m, 2H C_2H_4], 4.26 [s, 5H, Cp], 7.17−8.19 [m, 30H, Ph,-Py].

Anal. Calcd for $C_{42}H_{39}ClF_6FeN_3P_2PtSb$ (M_r = 1169.86): C, 43.12; H, 3.36; N, 3.51. Found: C, 43.78; H, 3.21; N, 3.34.

6a. A solution of **2a** (100 mg, 0.24 mmol), **3** (258 mg, 0.48 mmol), and $NaSbF_6$ (122 mg, 0.48 mmol) in methanol (100 mL) was heated to reflux for 36 h. The resulting red precipitate was washed three times with cold methanol and three times with ether and dried in vacuo. Recrystallization from CH_2Cl_2 by layering with ether afforded 156 mg (44%) of red, crystalline **6a**, mp 283 °C. ^{1}H NMR: 2.08−2.56 [m, 4H, C_2H_4], 4.56 [s, 5H, Cp], 7.25−7.45 [m, 20H, bpy, Ph], 7.87−7.94 [m, 6H, bpy, Ph], 8.42−8.47 [m, 2H, bpy].

Anal. Calcd for $C_{42}H_{37}ClF_6FeN_3P_2PtSb$ (M_r = 1167.84): C, 43.20; H, 3.19; N, 3.60. Found: C, 42.78; H, 3.11; N, 3.60.

6b: like **6a** from **2b** (86 mg, 0.19 mmol), **3** (210 mg, 0.38 mmol), and $NaSbF_6$ (100 mg, 0.38 mmol) in methanol (150 mL) for 68 h. Yield: 80 mg (33%) of **6b** as red-orange crystals, mp 284 °C. ^{1}H NMR: 2.10−2.79 [m, 4H, C_2H_4], 4.55 [s, 5H, Cp], 5.22 [s, 2H, CH_2Cl_2], 7.46−8.05 [m, 26H, phen, Ph], 8.96−9.02 [m, 2H, phen].

Anal. Calcd for $C_{44}H_{37}ClF_6FeN_3P_2PtSb\cdot CH_2Cl_2$ (M_r = 1191.86 + 84.93): C, 42.33; H, 3.08; N, 3.29. Found: C, 43.40; H, 3.02; N, 3.23.

7a: like **6a** from **2a** (100 mg, 0.24 mmol), **4** (170 mg, 0.24 mmol), and $NaSbF_6$ (61 mg, 0.24 mmol) in methanol (40 mL) for 5 h. Yield: 180 mg (60%) of **7a** as yellow microcrystals, mp 192 °C (dec). ^{1}H NMR: 4.60 [s, 5H, Cp], 7.10−9.52 [m, 38H, bpy, Ph].

Anal. Calcd for $C_{52}H_{43}ClF_6N_3P_2PtRuSb$ (M_r = 1339.22): C, 46.64; H, 3.24; N, 3.14. Found: C, 46.04; H, 3.34; N, 3.03.

8. A solution of **1** (40 mg, 0.095 mmol), **3** (140 mg, 0.26 mmol), and $NaSbF_6$ (48 mg, 0.19 mmol) in methanol (50 mL) was heated to reflux for 72 h. After cooling to room temperature and reduction of the volume to 20 mL in vacuo the solution was filtered. The precipitate was picked up in CH_2Cl_2 and filtered again. The filtrate was evaporated to dryness in vacuo and the residue dissolved in a minimum amount of acetone. Layering with ether afforded 60 mg (33%) of yellow, crystalline **8**, mp 291 °C (dec). ^{1}H NMR: 1.98−2.26 [m, 4H, C_2H_4], 4.36 [s, 10H, Cp], 7.27−8.08 [m, 50H, Py, Ph].

Anal. Calcd for $C_{74}H_{68}F_{12}Fe_2N_4P_4PtSb_2$ (M_r = 1915.52): C, 46.40; H, 3.58; N, 2.92. Found: C, 46.67; H, 3.42; N, 3.18.

9a. The CH_2Cl_2/ether solution remaining after the crystallization of **6a** (ca. 70 mL, see above) was reduced in vacuo to 25 mL and left to stand at room temperature for 4 days, during which time a red precipitate formed. This was filtered off, redissolved in 5 mL of CH_2Cl_2, and layered with 20 mL of petroleum ether (bp 60−70 °C) to afford 80 mg (18%) of red, crystalline **9a**, mp 230 °C (dec). ^{1}H NMR: 1.98−2.46 [m, 8H, C_2H_4], 4.33 [s, 10H, Cp], 7.20−7.50 [m, 40H, bpy, Ph], 7.81−7.91 [m, 6H, bpy, Ph], 8.22−8.28 [m, 2H, bpy].

Anal. Calcd for $C_{74}H_{66}F_{12}Fe_2N_4P_4PtSb_2$ (M_r = 1913.51): C, 46.45; H, 3.48; N, 2.93. Found: C, 46.63; H, 3.56; N, 2.90.

9b. The CH_2Cl_2/ether solution remaining after the crystallization of **6b** (ca. 60 mL, see above) was evaporated to dryness in vacuo. The residue was redissolved in CH_2Cl_2, filtered, and layered with 50 mL of petroleum ether (mp 60−70 °C), producing a red oily precipitate. This was dissolved in 20 mL of CH_2Cl_2 again and layered with 20 mL of cyclohexane, affording 140 mg (37%) of red, crystalline **9b**, mp 244 °C. ^{1}H NMR: 2.00−2.49 [m, 8H, C_2H_4], 4.35 [s, 10H, Cp], 7.26−7.95 [m, 46H, phen, Ph], 8.78−8.83 [m, 2H, phen].

Anal. Calcd for $C_{76}H_{66}F_{12}Fe_2N_4P_4PtSb_2$ (M_r = 1937.53): C, 47.11; H, 3.43; N, 2.89. Found: C, 46.31; H, 3.53; N, 2.86.

14. A solution of **10** (50 mg, 0.12 mmol) and **12** (150 mg, 0.26 mmol) in methanol (150 mL) was stirred for 4 h. Then the volume was reduced in vacuo to 50 mL. Upon addition of 64 mg (0.25 mmol) of $NaSbF_6$, an orange powder was precipitated. The supernatant solution was decanted and kept for the isolation of **15** (see below). The precipitate was washed three times with methanol and dried in vacuo. Dissolution in 10 mL of acetone and layering with 15 mL of ether afforded 80 mg (34%) of red, crystalline **14**, mp >300 °C (dec). ^{1}H NMR: 1.79−2.16 [m, 8H, C_2H_4], 4.27 [s, 10H, Cp], 7.13−7.99 [m, 50H, py, Ph].

Anal. Calcd for $C_{74}H_{68}F_{12}Fe_2N_4P_4PtSb_2$ (M_r = 1915.52): C, 46.40; H, 3.58; N, 2.92. Found: C, 46.22; H, 3.52; N, 2.90.

15. The supernatant solution from the preparation of **14** (see above) was evaporated to dryness in vacuo. Dissolution in 10 mL of CH_2Cl_2 and layering with 20 mL of ether afforded 30 mg (17%) of red, crystalline **15**, mp 239 °C. ^{1}H NMR: 2.05−2.50 [m, 4H, C_2H_4], 3.85 [s, 5H, Cp], 7.05−7.85 [m, 40H, Ph].

Anal. Calcd for $C_{59}H_{53}F_6FeN_2PtSb$ (M_r = 1400.64): C, 50.59; H, 3.81; N, 2.00. Found: C, 49.83; H, 3.82; N, 2.10.

16. A solution of **11** (25 mg, 0.06 mmol) and **13a** (99 mg, 0.12 mmol) in methanol (100 mL) was heated to reflux for 20 min. The solvent was removed in vacuo and the residue extracted three times with 10 mL portions of CH_2Cl_2. The solution was filtered and layered with 30 mL of petroleum ether (bp 60−70 °C), affording 40 mg (33%) of purple, crystalline **16**, mp >300 °C (dec). ^{1}H NMR: 2.43−2.79 [m, 8H, C_2H_4], 4.16 [s, 10H, Cp], 7.07−8.35 [m, 48H, bpy, Ph].

Anal. Calcd for $C_{74}H_{66}F_{12}Fe_2N_4P_4PtSb_2$ (M_r = 1913.51): C, 46.45; H, 3.48; N, 2.93. Found: C, 45.56; H, 3.29; N, 2.83.

20. A solution of **17** (500 mg, 0.36 mmol) and **13b** (460 mg, 0.72 mmol) in CH_2Cl_2 (200 mL) was stirred for 3 days. After reduction of

(29) Kauffman, G. B. *Inorg. Synth.* **1963**, *7*, 249−253.
(30) Morgan, G. T.; Burstall, F. H. *J. Chem. Soc.* **1934**, 965−971.
(31) Hodges, K. D.; Rund, J. V. *Inorg. Chem.* **1975**, *14*, 525−528.
(32) Cattalini, L.; Guidi, F.; Tobe, M. L. *J. Chem. Soc., Dalton Trans.* **1993**, 233−236.
(33) Che, C. M.; He, L. Y.; Poon, C. K.; Mak, T. C. W. *Inorg. Chem.* **1989**, *28*, 3081−3083.
(34) Martinsen, A.; Sonstad, J. *Acta Chem. Scand.* **1977**, *A31*, 645−650.

Table 6. Electronic Spectra of Complexes and Their Oxidation Products[a]

complex	λ_{max} (ϵ) (nm, L mol^{-1} cm^{-1})
5	241 (9020), 257 (8930), 268 (8930), 330 sh (2840), 386 sh (1120)
[**5**]$^+$	241 (9260), 257 (9090), 268 (9110), 301 sh (6370), 380 sh (1780)
14	248 (35 300), 262 (35 400), 304 (18 600), 368 (9260), 484 (1990)
[**14**]$^+$	248 (35 600), 262 (35 800), 304 (30 900), 368 sh (10 350), 450 (6820), 1313 (560)
[**14**]$^{2+}$	248 (35 800), 262 (36 000), 304 (36 200), 368 (16 700), 450 (9620)
16	244 (17 800), 268 (17 900), 292 (15 600), 316 (17 400), 368 (3590), 480 (2250), 520 (3510)
16/[**16**]$^{2+}$	244 (17 900), 268 (17 900), 292 (17 300), 316 (17 900), 368 (4540), 440 (4740), 480 (3450), 520 (3010)
[**16**]$^{2+}$	244 (18 400), 268 (17 900), 292 (18 500), 316 (18 400), 368 (7440), 444 (3700)
20	326 (10 400), 341 (10 700), 466 (1360)
[**20**]$^+$	312 (12 200), 322 (11 700), 341 (10 400), 450 (3990), 1560 (600)
[**20**]$^{2+}$	308 (12 500), 324 (12 200), 341 (12 300), 442 (7420)
22	236 (4070), 347 (4380), 374 (3680), 441 sh (740)
[**22**]$^+$	236 (4510), 347 (4470), 374 (3990), 441 sh (3000), 750 (270)

[a] In CH_2Cl_2.

the volume to 5 mL in vacuo it was chromatographed over a 2 × 30 cm silica gel column with CH_2Cl_2/acetone (5:2). Complex **20** was contained in the first, red band. Recrystallization from 20 mL of CH_2Cl_2 layered with 20 mL of petroleum ether (bp 60−70 °C) afforded 350 mg (72%) of red, crystalline **20**, mp 192 °C. ^{1}H NMR: 2.10−2.42 [m, 8H, C_2H_4], 4.10 [s, 10H, Cp], 5.22 [s, 2H, CH_2Cl_2], 7.12−7.72 [m, 40H, Ph].

Anal. Calcd for $C_{66}H_{58}Fe_2N_4P_4Pt{\cdot}CH_2Cl_2$ (M_r = 1337.88 + 84.93): C, 56,56; H, 4.25; N, 3.94. Found: C, 56.37, H, 4.20; N, 3.91.

21. A solution of **17** (95 mg, 0.069 mmol) and **19** (100 mg, 0.138 mmol) in methanol (30 mL) was heated to reflux for 30 min. After cooling to room temperature the precipitate was filtered off and washed with three 10 mL portions of methanol. Dissolving in ca. 100 mL of boiling CH_2Cl_2 and cooling in a refrigerator yielded 55 mg (45%) of yellow, crystalline **21**, mp 193 °C. ^{1}H NMR: 3.56 [s, 10H, Cp], 5.26 [s, 2H, CH_2Cl_2], 7.18−7.87 [m, 60H, Ph].

Anal. Calcd for $C_{86}H_{70}N_4P_4PtRu_2{\cdot}CH_2Cl_2$ (M_r = 1680.64 + 84.93): C, 59.19; H, 4.11; N, 3.17. Found: C, 59.99; H, 4.21; N, 3.17.

22. A solution of **12** (262 mg, 0.44 mmol) in methanol (100 mL) was added dropwise with stirring over a period of 5 h to a solution of **17** (600 mg, 0.44 mmol) in methanol (40 mL). Then solid **19** (350 mg, 0.48 mmol) was added and the mixture heated to reflux for 20 min. Filtration of the warm solution removed a precipitate of 40 mg (5%) of **21**. After addition of 100 mg of **19** the mixture was left to stand at room temperature for 18 h. The resulting precipitate was filtered off, dissolved in a minimum amount of CH_2Cl_2, and chromatographed over a 2 × 30 cm silica gel column with CH_2Cl_2/acetone (5:2). The first, red, band yielded 120 mg (20%) of **20**. From the second, orange, band after evaporation to dryness remained 100 mg (15%) of **22** as an orange-red powder, mp 164 °C. ^{1}H NMR: 2.17−2.78 [m, 4H, dppe], 3.59 [s, 5H, Cp], 4.21 [s, 5H, Cp], 5.29 [s, 2H, CH_2Cl_2], 7.14−7.85 [m, 50H, Ph].

Anal. Calcd for $C_{76}H_{64}FeN_4P_4PtRu{\cdot}CH_2Cl_2$ (M_r = 1509.26 + 84.93): C, 58.01; H, 4.17; N, 3.51. Found: C, 58.11; H, 4.23; N, 3.51.

23. A solution of **1** (20 mg, 0.047 mmol) and **18a** (86 mg, 0.047 mmol) in CH_2Cl_2 (50 mL) was heated to reflux for 3 h. After reduction of the volume to 10 mL in vacuo and layering with 30 mL of ether, 20 mg (25%) of green, crystalline **23**, mp 198 °C (dec), was obtained.

Anal. Calcd for $C_{88}H_{70}ClFeN_{10}P_4Pt{\cdot}CH_2Cl_2$ (M_r = 1677.86 + 84.93): C, 60.64; H, 4.12; N, 7.95. Found: C, 60.64; H, 4.05; N, 7.74.

24. A solution of **1** (20 mg, 0.047 mmol) and **18b** (92 mg, 0.095 mmol) in methanol (100 mL) was heated to reflux for 36 h. After evaporation to dryness the residue was picked up in 10 mL of CH_2Cl_2,

Table 7. Crystallographic Data

	5	**6a**	**8**·2 acetone	**9a**·1/2CH_3OH	**14**	**16**	**20**·CH_2Cl_2
formula	$C_{42}H_{39}ClF_6FeN_3P_2PtSb$	$C_{42}H_{37}ClF_6FeN_3P_2PtSb$	$C_{86}H_{92}F_{12}Fe_2N_4O_4P_4PtSb_2$	$C_{74.5}H_{68}F_{12}Fe_2N_4O_{0.5}P_4PtSb_2$	$C_{74}H_{68}F_{12}Fe_2N_4P_4PtSb_2$	$C_{74}H_{66}F_{12}Fe_2N_4P_4PtSb_2$	$C_{64}H_{60}Cl_2Fe_2N_4P_4Pt$
MW	1169.9	1167.8	2147.8	1929.5	1915.5	1913.5	1422.8
space group	*P*1	$P2_1/c$	*P*1	*P*1	*C*2/*c*	$P6_1$	$P2_1/c$
Z	2	4	1	4	4	6	2
a (Å)	12.074(2)	13.047(3)	11.846(2)	14.796(3)	31.215(6)	32.120(6)	13.399(3)
b (Å)	12.220(2)	15.018(3)	11.918(2)	18.158(4)	11.384(2)	32.120(6)	14.598(3)
c (Å)	15.434(3)	21.660(4)	15.130(3)	32.363(6)	25.738(5)	14.460(3)	15.895(3)
α (deg)	80.89(3)	90	95.03(3)	88.43(3)	90	90	90
β (deg)	88.36(3)	101.77(3)	91.25(3)	84.34(3)	123.09(3)	120	101.15(3)
γ (deg)	79.76(3)	90	94.73(3)	72.83(3)	90	90	90
V (Å^3)	2212.7(7)	4155(2)	2119.7(7)	8267(3)	7663(2)	12920(4)	3050.4(2)
d(calc) [g cm^{-3}]	1.75	1.87	1.68	1.49	1.66	1.48	1.55
μ(Mo Kα) (mm^{-1})	4.23	4.55	2.76	2.70	3.04	2.70	2.99
R1 (obs reflns)[a]	0.057	0.032	0.040	0.098	0.041	0.064	0.039
wR2 (all reflns)[b]	0.162	0.087	0.111	0.285	0.106	0.157	0.106

[a] $R1 = \sum|F_o - F_c|/\sum F_o$. [b] $wR2 = [\sum[w(F_o^2 - F_c^2)^2]/\sum[w(F_o^2)^2]]^{1/2}$.

the suspension was filtered, and the filtrate was layered with 20 mL of petroleum ether (bp 60−70 °C). After one day a yellow oil had formed. This was redissolved in 15 mL of CH_2Cl_2, which was layered with 20 mL of ether, affording 16 mg (20%) of yellow, crystalline **24**, mp 215 °C.

Anal. Calcd for $C_{86}H_{154}Fe_2N_{18}Pt\cdot CH_2Cl_2$ (M_r = 1747.06 + 84.93): C, 57.04; H, 8.58; N, 13.76. Found: C, 57.29; H, 8.49; N, 13.90.

Chemical Oxidations. The complexes (typically 10−20 mg) were dissolved in degassed CH_2Cl_2 and diluted to a concentration suitable for the UV−vis−near-IR spectrometer. The oxidant was added as a solid in 1 mg portions. The color of the solutions darkened progressively. After each addition a spectrum was recorded. Attempts to isolate the oxidation products were made after the addition of 1 or 2 equiv of the oxidant, respectively. For this purpose precipitation was either induced by addition of petroleum ether or performed slowly by layering with petroleum ether or ether. While IR and UV−vis−near-IR spectroscopy of the solutions indicated that they contain mostly the desired oxidation products, the precipitates from these solutions were neither analytically pure nor completely soluble in CH_2Cl_2 again. Table 6 lists the UV−vis−near-IR data of the starting complexes and of their one- and two-electron oxidation products.

Structure Determinations. Crystals were taken from the isolated compounds without further recrystallization. They were sealed in glass capillaries. Diffraction data were recorded at room temperature on a Nonius CAD4 diffractometer with graphite-monochromatized Mo Kα radiation (λ = 0.7107 Å), except for **9a** and **16**, which were measured on a Stoe IPDS diffractometer at −50 °C. Empirical absorption corrections based on ψ scans were applied except for **9a** and **16**, where this was not possible due to the image plate technique. The structures were solved with direct methods and refined anisotropically with the SHELX program suite.[35] Hydrogen atoms were included with fixed distances and isotropic temperature factors 1.2 times those of their attached atoms. Parameters were refined against F^2. The crystal used for the structure determination of **5**, obtained after an extended period of crystallization, was found to have significant amounts of Pt-bound Cl^- replaced by CN^-, i.e., it showed Pt−Cl/Pt−CN disorder (see Supporting Information for details). **9a** has two independent formula units per asymmetric unit and was found to have a 7:1 disorder of SbF_6 and Cl counterions. Drawings were produced with SCHAKAL.[36] Table 7 lists the crystallographic data.

Acknowledgment. This work was supported by the European Commission and by the Graduiertenkolleg "Ungepaarte Elektronen" of the Deutsche Forschungsgemeinschaft. We are indebted to Prof. D. Fenske and Dr. H. Gösmann, Karlsruhe, for obtaining the X-ray data sets of **9a** and **16** and to Dr. K. Weis for help with the structure determinations.

Supporting Information Available: Fully labeled ORTEP plots to accompany the seven molecular structures and cyclic and square-wave voltammograms of complexes **14** and **20**. X-ray crystallographic files in CIF format. This material is available free of charge via the Internet at http://pubs.acs.org.

IC981384L

(35) Sheldrick, G. M. *SHELXS-86* and *SHELXL-93*; Universität Göttingen: Göttingen, 1986 and 1993.
(36) Keller, H. J. *SCHAKAL for Windows*; Universität Freiburg: Freiburg, 1997.